

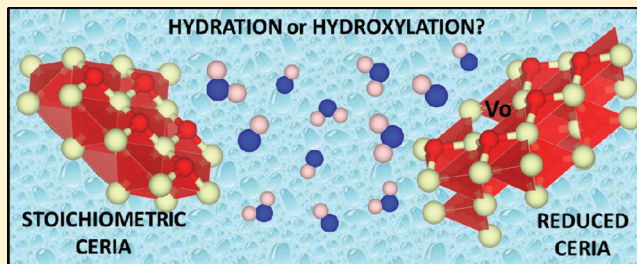
# Water Adsorption and Its Effect on the Stability of Low Index Stoichiometric and Reduced Surfaces of Ceria

Marco Molinari,<sup>†</sup> Stephen C. Parker,<sup>\*,†</sup> Dean C. Sayle,<sup>‡</sup> and M. Saiful Islam<sup>†</sup>

<sup>†</sup>Department of Chemistry, University of Bath, Claverton Down, Bath, Avon, BA2 7AY, U.K.

<sup>‡</sup>Department of Engineering and Applied Science, Cranfield University, Defence Academy of the United Kingdom, Shrivenham, SN6 8LA, U.K.

**ABSTRACT:** The influence of water on the redox properties of ceria is pivotal to its widespread exploitation spanning a variety of applications. *Ab initio* simulation techniques based on DFT-GGA+U are used to investigate the water–ceria system including associative ( $H_2O$ ) and dissociative ( $-OH$ ) adsorption/desorption of water and the formation of oxygen vacancies in the presence of water vapor on the stoichiometric and reduced low index surfaces of ceria at different water coverages. Our calculations address the controversy concerning the adsorption of water on the  $CeO_2\{111\}$ , and new results are reported for the  $CeO_2\{110\}$  and  $\{100\}$  surfaces. The simulations reveal strong water coverage dependence for dissociatively ( $-OH$ ) adsorbed water on stoichiometric surfaces which becomes progressively destabilized at high coverage, while associative ( $H_2O$ ) adsorption depends weakly on the coverage due to weaker interactions between the adsorbed molecules. Analysis of the adsorption geometries suggests that the surface cerium atom coordination controls the strong adhesion of water as the average distance  $Ce-O_W$  is always 10% greater than the  $Ce-O$  distance in the bulk, while the hydrogen bonding network dictates the orientation of the molecules. The adsorption energy is predicted to increase on reduced surfaces because oxygen vacancies act as active sites for water dissociation. Crucially, by calculating the heat of reduction of dry and wet surfaces, we also show that water promotes further reduction of ceria surfaces and is therefore central to its redox chemistry. Finally, we show how these simulation approaches can be used to evaluate water desorption as a function of temperature and pressure which accords well with experimental data for  $CeO_2\{111\}$ . We predict desorption temperatures ( $T_D$ ) for  $CeO_2\{110\}$  and  $CeO_2\{100\}$  surfaces, where experimental data are not yet available. Such an understanding will help experiment interpret the complex surface/interface redox processes of ceria, which will, inevitably, include water.



## 1. INTRODUCTION

Ceria ( $CeO_2$ ) and ceria-based materials are valuable fluorite-structured oxides with remarkable redox properties for technological applications. In particular, ceria is exploited in oxidative catalysis,<sup>1–3</sup> sensors,<sup>4</sup> glass polishing,<sup>5,6</sup> solid oxide fuel cells (SOFC),<sup>7–9</sup> and biomedical technology (free radical scavenger)<sup>10,11</sup> where catalytically active surfaces and high ionic conductivity are pivotal. The wide range of applications is driven by ceria's ability to store and release oxygen (by creating oxygen vacancies) due to the easily accessible oxidation states of cerium ions ( $Ce^{3+}$  and  $Ce^{4+}$ ).

One of the outstanding challenges is to understand the role of surface structure and composition on the various applications, as it is well-known that surface and interface events govern  $CeO_2$  functionality. Zhang et al.<sup>12</sup> have shown for instance that ceria nanocubes, bounded by six  $\{100\}$  surfaces, enable low-temperature oxygen storage capacity (OSC). OSC occurs at 150 °C without active species loading which is 250 °C lower compared to irregular shaped  $CeO_2$  supporting the view that such nanocubes, also previously reported in the literature,<sup>13,14</sup> have great potential as low-temperature catalysts. In many applications, however, water

adsorption is an unavoidable process, as water is present either as a reactant or spectator. The adsorption mechanism as well as the wetting behavior is driven by a complex interplay of factors such as the surface geometry and the energetics and kinetics associated with the adsorption.

The most controversial issue about the water–ceria interaction is the possibility that ceria may concurrently support reduction and oxidation of the same molecule (in this case water) depending on the orientation and the structural elements of the surface. This behavior becomes intriguing when moving to the nanometre scale due to the decrease in the volume/area ratio, and might imply electronic defects flow between different surfaces of the same size-limited particle. Several early experiments suggested that  $H_2O$  promotes oxidation of reduced ceria thin films<sup>15–17</sup> but also that water favors further reduction of a reduced ceria thin film on Pt(111).<sup>18</sup>

**Received:** January 17, 2012

**Revised:** February 29, 2012

**Published:** February 29, 2012

Hayun et al.<sup>19</sup> used water adsorption calorimetry to calculate the surface enthalpy of the hydrated surface and the water adsorption enthalpy for a nanoceria sample with crystalline quasi-spherical size particles of about 4 nm and with Ce<sup>3+</sup> ion concentration of about 1%, finding that 8.79 H<sub>2</sub>O/nm<sup>2</sup> coverage is the transition coverage from chemisorbed to physisorbed water with an adsorption enthalpy for chemisorbed water of -59.82 kJ/mol. Two sites for H<sub>2</sub>O adsorption are identified in agreement with previous investigations;<sup>20,21</sup> site 1 (s1) is above Ce<sup>4+</sup> ions and site 2 (s2) is above the oxygen vacancies (Vo) with adjacent Ce<sup>3+</sup> ions and with possible formation of hydroxide. The water gas shift reaction (WGS) was investigated on an inverse CeO<sub>x</sub>/Au(111) catalyst, confirming that the presence of Ce<sup>3+</sup> leads to dissociation of H<sub>2</sub>O to form OH groups which are stable up to 600 K.<sup>22</sup>

Despite providing valuable data, these studies are not ideal for extracting a reliable correlation between surface structure and surface chemistry due to the variety of surface terminations expressed by (nano)ceria powders in one case, and the lattice mismatch, the substoichiometry,<sup>23</sup> and the interference of the noble metal substrate with ceria surface chemistry in the other. More convenient for this purpose are investigations on specific Miller index surfaces. A combined XPS–TPD study<sup>24</sup> reported further reduction mediated by water rather than oxidation of reduced CeO<sub>2</sub>(111) surface with enhancement of oxygen vacancies (Vo) concentration in the presence of water vapor more likely due to bulk-to-surface diffusion of Vo rather than removal of lattice oxygen via O<sub>2</sub> desorption. The authors also reported strong water coverage dependence on the oxidized but not on the reduced CeO<sub>2</sub>(111) surface. SFM experiments<sup>21</sup> have shown the coexistence of Vo, adsorbed H<sub>2</sub>O above cerium ions and hydroxide substituting surface oxygen on the reduced CeO<sub>2</sub>(111) surface. Vo can act as centers for H<sub>2</sub>O dissociation under reducing conditions even though water is not necessarily dissociated. Further investigations<sup>20</sup> found also strong water–ceria interaction on the stoichiometric CeO<sub>2</sub>(111) surface with no significant hydrogen bonding occurring between adsorbates. These observations seem to rule out dissociation of water even though the authors suggested that H<sub>2</sub>O can be either molecularly adsorbed or dissociated with the proton close to the hydroxide to preserve local charge neutrality. XPS and TPD were used to investigate the stoichiometric CeO<sub>2</sub>(111)/Cu(111) model catalyst, revealing the presence of water molecularly adsorbed on the surface up to 120 K and coadsorbed water/hydroxide above 200 K.<sup>25</sup> H<sub>2</sub>O dissociation was found to be more pronounced on the reduced surface with the Ce<sup>3+</sup>/Ce<sup>4+</sup> ratio increasing due to the presence of water fragments.

Theoretical calculations have also been valuable for understanding water–ceria interactions. Early *ab initio* calculations using DFT-GGA investigated water adsorption on a stoichiometric and reduced CeO<sub>2</sub>(111) (2 × 1) surface unit cell,<sup>26</sup> finding weak coverage dependence in disagreement with the experiments of Henderson et al.<sup>24</sup> Water adsorbs with a single H bond above Ce<sup>4+</sup> in both clean and reduced surface. Oxidation of the reduced surface led by water dissociation and evolution of H<sub>2</sub> is also found to be slightly energetically favorable. Adsorption of H<sub>2</sub>O in a single H bond configuration was reported on the stoichiometric CeO<sub>2</sub>(111) surface by Yang et al.,<sup>27</sup> while both associatively (no H bonds) and dissociatively adsorbed molecules are present on the reduced surface. The double H bond adsorption geometry was also simulated and found to be the most stable.<sup>28–30</sup> DFT-GGA+U

calculations confirmed the dissociative behavior of water not only on the reduced but also on the stoichiometric CeO<sub>2</sub>(111) (2 × √2) surface.<sup>31</sup> *Ab initio* MD on the reduced surface suggested also that the energy barrier for water dissociation is very small,<sup>30,31</sup> also leading to the controversial issue that the presence of Ce<sup>3+</sup> does not imply the existence of Vo.<sup>24,25</sup> A DFT-GGA study<sup>29</sup> reported associatively adsorbed water on the stoichiometric CeO<sub>2</sub>(111) (2 × 2) surface, while associatively adsorbed H<sub>2</sub>O is thermodynamically stable but kinetically unlikely on the reduced surface which, however, disagrees with the presence of hydroxide seen by experiments.<sup>21,25</sup> The discrepancy on the dissociation of water on the reduced CeO<sub>2</sub>(111) surface between Fronzi et al.<sup>29</sup> and Watkins et al.<sup>31</sup> and Marrocchelli et al.<sup>30</sup> has recently been addressed by the latter.

Considering the above literature, it is clear that the ceria–water interaction is far from understood. Therefore, the aim of the present paper is to use DFT-based electronic structure methods to elucidate the redox properties of the stoichiometric and reduced low index ceria surfaces in the presence of associatively and dissociatively adsorbed water. Here we revisit the thermodynamics of the adsorption of water on the CeO<sub>2</sub>{111} surface and present new studies on the adsorption of water on the {110} and {100} surfaces in the light of a recent proposal of active ceria surfaces for low-*T* catalysis.<sup>12</sup> We explore for the first time how H<sub>2</sub>O and hydroxide adsorb onto these reactive surfaces at the atomistic level, as this is the first step in understanding the mechanism underpinning the catalytic behavior of CeO<sub>2</sub> surfaces. Finally, since the thermodynamic stability of ceria surfaces is affected by the surrounding environment, we examine the temperatures of desorption for water in a range of different pressures. The simulation results will be compared and validated against the available experimental data.

## 2. METHODOLOGY

Calculations were performed using the VASP code,<sup>32,33</sup> in which the valence electronic states are expanded in the basis of plane waves, with the core–valence interaction represented using the projector augmented wave (PAW) approach.<sup>34,35</sup> The frozen core is [He] for oxygen and [Xe] for cerium. The exchange correlation functional applied was the Perdew–Burke–Ernzerhof (PBE) GGA<sup>36</sup> with the inclusion of the Hubbard-U term using the Dudarev approach.<sup>37</sup> The GGA+U methodology<sup>38</sup> enables the approach to account for the presence of the localized Ce<sup>3+</sup> states. The sensitivity of results to the U parameter for GGA+U calculations on ceria has been described in the literature, where a U value of 5 eV was chosen for the Ce f orbitals.<sup>39–43</sup> 3D boundary conditions were used throughout, and hence, the surfaces were modeled using the slab method<sup>44</sup> in which a finite number of crystal layers is used to generate two identical surfaces via the introduction of a vacuum gap perpendicular to the surface. A vacuum gap of 15 Å was used to minimize the interaction between images. The {100} and {110} slabs with a p(2 × 2) expansion of the surface unit cell included 13 and 7 atomic layers (24 and 28 CeO<sub>2</sub> units, respectively), while the {111} slab with a p(2 × 3) expansion included 12 atomic layers (24 CeO<sub>2</sub> units). The cutoff energy for the plane wave basis was 500 eV with the Brillouin zone sampled using a 2 × 2 × 1 Monkhorst–Pack grid, with the third vector perpendicular to the surface plane. All calculations were spin polarized, and relaxation of the atomic structure for all atoms was deemed to have converged when the

forces were below 0.01 eV Å<sup>-1</sup>. All slab calculations use symmetric introduction of oxygen vacancies and adsorbates on both sides of the slab, thus ensuring that the surfaces were identical and the cell had no net dipole moment. As the number of configurations for adsorbed water on surfaces of ceria is extremely large, we have limited the choice to structures that have previously been suggested and that maximize the hydrogen bonding between the adsorbate and the surface. Few configurations for the lowest water coverage were then computed, but only the most stable one is reported. This configuration was then kept for water molecules when high water coverage was studied. All figures were drawn using the program VESTA.<sup>45</sup>

### 3. RESULTS AND DISCUSSION

We start by presenting the energetics of the stoichiometric (section 3.1) followed by the reduced low index ceria surfaces (section 3.2). The adsorption of water on the stoichiometric surfaces is described considering first the associative state (section 3.3.1) followed by the dissociative state (section 3.3.2) at the lowest coverage. The coverage dependence of the energetics of associative adsorption is discussed for the {111} surface separately (section 3.3.3) from the {100} and {110} surfaces (section 3.3.4) because of the availability of experimental and computational data for comparison. The coverage dependence within the dissociative adsorption (section 3.3.5) is presented followed by the comparison between the different behavior of associatively and dissociatively adsorbed water (section 3.3.6) on the stoichiometric surfaces. The adsorption of H<sub>2</sub>O on reduced surfaces (section 3.4) and the heat of reduction of ceria surface in the presence of water (section 3.5) are presented before discussing the thermodynamics of desorption (section 3.6).

**3.1. Stoichiometric {100}, {110}, and {111} Ceria Surfaces.** We have investigated the three low index oxygen terminated surfaces of ceria: type I {110}, type II {111}, and type III {100} surfaces according to Tasker classification.<sup>46</sup> The dipole moment normal to the surface vector of the type III surfaces was quenched by moving half of the surface oxygen atoms from one side to the other of the slab.<sup>47</sup> The slabs were generated from a relaxed bulk unit cell with a lattice constant of 5.489 Å which compares well with the experimental value of 5.411 Å<sup>48</sup> and with previous theoretical work.<sup>40,49</sup> The relative stability of the relaxed surfaces increases in the order {100}, {110}, and {111} with values of 90, 67, and 44 meV Å<sup>-2</sup> (1.44, 1.06, 0.71 J m<sup>-2</sup>), respectively, which agrees with previously calculated surface energies<sup>40,49</sup> and is consistent with the order of surface stability from other atomistic simulation studies of ceria.<sup>50–54</sup>

**3.2. Reduced {100}, {110}, and {111} Ceria Surfaces.** The heat of reduction of the three low index surfaces of ceria was investigated by creating oxygen vacancies upon removal of oxygen ions while two electrons are left in the lattice localized on the cerium ions neighboring the vacancy. The heat of reduction ( $E_{\text{red}}$ ) is calculated as in eq 1 where  $E(\text{CeO}_{2-x})$  and  $E(\text{CeO}_2)$  are the energies of the reduced and stoichiometric slabs and  $E(\text{O}_2)$  is the binding energy of the O<sub>2</sub> gas phase molecule in its triplet state.

$$E_{\text{red}} = [E(\text{CeO}_{2-x}) + E(\text{O}_2) - E(\text{CeO}_2)]/2 \quad (1)$$

Computed values for the heat of reduction of bulk ceria depend on the DFT methodology and the size of the simulation cell.<sup>40,41,43,55,56</sup> Using a 2 × 2 × 2 (96 atoms) supercell with the

Brillouin zone sampled using a 2 × 2 × 2 Monkhorst–Pack grid, we calculated the heat of reduction for bulk ceria to be 2.63 eV which compares well with Keating et al.<sup>41</sup> (2.11 eV) and Scanlon et al.<sup>43</sup> (2.62 eV) but is lower than Nolan et al.<sup>56</sup> (3.39 eV) and the experimental value of 4.67 eV reported by Tuller et al.<sup>57</sup>

We have also calculated the heat of reduction for the {111}, {100}, and {110} surfaces to be 2.01, 1.61, and 1.29 eV, respectively. As expected, these are lower than the bulk value which supports the experimental observation that ceria surfaces are more reactive than the bulk. Overall, the order of stability is the same as has been reported in the literature, but quantitatively the values are lower.<sup>39,41,55</sup> Interestingly, the order in energy does not follow the order of stability of pure surfaces. The most stable {111} surface has the highest heat of reduction as expected; however, the lowest is not associated with the least stable {100} surface but with the {110} surface.

**3.3. Water Adsorption on Stoichiometric {100}, {110}, and {111} Ceria Surfaces.** We next considered the structure and energetics of the associative and dissociative adsorption of water on stoichiometric ceria surfaces for different water coverages. The adsorption energy ( $E_{\text{ads}}$ ) is calculated as in eq 2, where  $E_{(\text{slab+mol})}$  and  $E_{(\text{slab})}$  are the energies of the slab with the adsorbed molecule and the clean slab, respectively, and  $E_{(\text{mol})}$  is the energy of the molecule in the gas phase.

$$E_{\text{ads}} = [E_{(\text{slab+mol})} - (E_{(\text{slab})} + n_{(\text{mol})}E_{(\text{mol})})]/n_{(\text{mol})} \quad (2)$$

To discriminate between physisorption and chemisorption, we use a value of −0.6 eV according to Hayun et al.,<sup>19</sup> and to indicate the water molecule associatively and dissociatively adsorbed at the surface, we refer to associative and dissociative state.

**3.3.1. Associative State at the Lowest Coverage.** The lowest water coverage considered was 1.66, 1.17, and 1.28 H<sub>2</sub>O/nm<sup>2</sup> for the p(2 × 2) {100}, p(2 × 2) {110}, and p(2 × 3) {111} expanded surfaces, respectively, and occurs when a single water molecule adsorbs on the surface. The adsorption energies (Table 1) for the associatively adsorbed water at the

**Table 1. Adsorption Energies of Associatively (H<sub>2</sub>O) and Dissociatively (H–OH) Adsorbed Water on Stoichiometric Ceria Surfaces at Different Water Coverages (H<sub>2</sub>O/nm<sup>2</sup>) (\*1HB and \*2HB)**

Adsorption Energy (eV)				
	coverage	1.66	3.32	6.64
{100}	H–OH	−1.57	−1.73/−0.87	−0.89
	H <sub>2</sub> O	−1.00		−0.89
{110}	H–OH	−1.12	−1.00	−0.21
	H <sub>2</sub> O	−0.85	−0.76	
{111}	coverage	1.28	3.83	7.67
	H–OH	−0.59		−0.15
	H <sub>2</sub> O	−0.58 <sup>§</sup> (−0.56*)	−0.60	−0.57

lowest water coverage are −1.00, −0.85, and −0.58 eV for the {100}, {110}, and {111} surfaces, respectively. The ordering of the energies follows that of the surface stability of pure surfaces.

Adsorption of water on the {111} surface has been discussed in the literature, while no specific study has been reported for the {100} and {110} surfaces to our knowledge. In our

calculations, associatively adsorbed water at the  $\{111\}$  surface has two energetically equivalent configurations ( $\Delta E = 0.02$  eV) with two H bonds (2HB,  $E_{\text{ads}} = -0.56$  eV) (Figure 1e) and

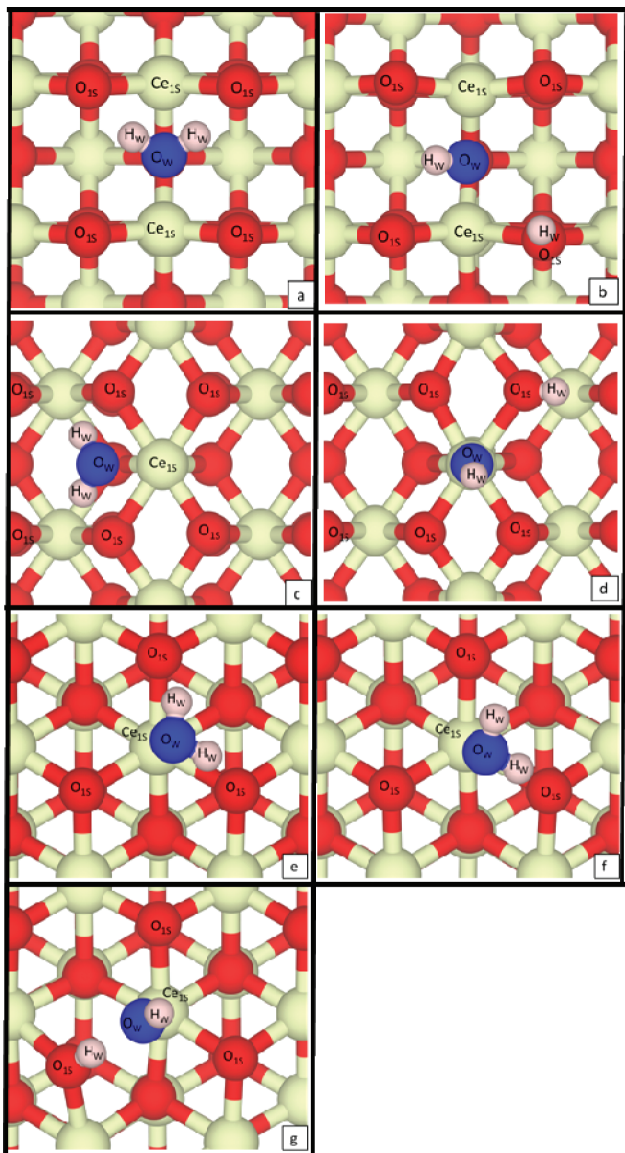


**Figure 1.** Top view of the adsorption site of associatively adsorbed water on (a)  $\{100\}$ , (c)  $\{110\}$ , and (e and f)  $\{111\}$  and dissociatively adsorbed water (b)  $\{100\}$ , (d)  $\{110\}$ , and (g)  $\{111\}$  stoichiometric ceria surfaces. White, red, pink, and blue spheres are Ce, O,  $\text{H}_W$ , and  $\text{O}_W$  atoms, respectively.

with one H bond (1HB,  $E_{\text{ads}} = -0.58$  eV) (Figure 1f); we infer that they are both in agreement with the SFM images at room temperature,<sup>21</sup> as the resolution of those images does not discriminate between the two configurations. The 2HB and 1HB configurations have been previously studied using *ab initio* calculations, but the order of stability is still unclear. In some investigations, 2HB was found to be the most stable with an adsorption energy of  $-0.49$  eV (0.25 ML),<sup>29</sup> of  $-0.52$  eV,<sup>28</sup> and of  $-0.51$  eV,<sup>30</sup> while in others the 1HB was claimed to be the lowest energy structure with an adsorption energy of  $-0.58$  eV (0.5 ML) and  $-0.55$  eV (1 ML)<sup>26</sup> and of  $-0.57$  eV (0.25 ML).<sup>27</sup>

Figure 1 depicts the adsorption geometries of a single water molecule on the low index ceria surfaces, and Table 2 reports

**Table 2. Most Significant Distances for the Associative and Dissociative States of Water at the Stoichiometric Ceria Surfaces (\*Two H Bonds;  $^{\$}$ Additional Distance;  $^{\text{I}}$ H Bonds)**

distance (Å)	associatively adsorbed water			
	$\{100\}$	$\{110\}$	1HB $\{111\}$	2HB $\{111\}$
$\text{H}_W-\text{O}_{1S}^{\text{Y}}$	2.11–1.97*	2.07*	1.68 (2.80 $^{\$}$ )	1.99–2.13*
$\text{Ce}_{1S}-\text{O}_W$	2.64–2.70	2.67	2.60	2.62
dissociatively adsorbed water				
distance (Å)	$\{100\}$		$\{110\}$	$\{111\}$
	$\text{Ce}_{1S}-\text{O}_W\text{H}_W$	2.34–2.37	2.14	2.22
$\text{Ce}_{1S}-\text{O}_{1S}\text{H}_W$	2.36–2.45	2.48–2.58	2.41	
$\text{H}_W-\text{O}_{1S}^{\text{Y}}$	2.52			
$\text{O}_{1S}\text{H}_W-\text{O}_{1S}^{\text{Y}}$		1.92		
$\text{O}_{1S}\text{H}_W-\text{O}_W\text{H}_W^{\text{Y}}$				1.65

the most significant distances between surface atoms and adsorbates. The following abbreviations are used in the text to describe the structures:  $\text{O}_{1S}$  and  $\text{O}_{2S}$  are the oxygen atoms in the first and second atomic layers,  $\text{Ce}_{1S}$  are the cerium atoms in the first atomic layer,  $\text{O}_W$  and  $\text{H}_W$  are the oxygen and hydrogen of water, and OH is the generic hydroxide. The adsorbed water orientates with the  $\text{H}_W$  pointing  $28^\circ$  outward from the surface plane on the  $\{100\}$  surface while  $50^\circ$  and  $14^\circ$  inward for the  $\{110\}$  and  $\{111\}$  surfaces, respectively. The position of the  $\text{H}_2\text{O}$  on the three surfaces can be related to the coordination sphere of the surface cerium ions. At the  $\{111\}$  surface, the position above  $\text{Ce}_{1S}$  is the only empty oxygen site available to  $\text{H}_2\text{O}$  to fully restore the 8-fold coordination of the cation.  $\text{Ce}_{1S}$  at the  $\{110\}$  and the  $\{100\}$  is 6-coordinated, and therefore, there are two available equivalent positions for the adsorption, but while for the  $\{110\}$  surface  $\text{O}_W$  will belong to the coordination sphere of one Ce (Figure 1c), for the  $\{100\}$  surface,  $\text{O}_W$  will be shared between two  $\text{Ce}_{1S}$  (Figure 1a). Interestingly, at the lowest water coverage, the distance  $\text{Ce}_{1S}-\text{O}_W$  is always between 2.60 and 2.70 Å, which is over 10% greater than the Ce–O distance in the bulk (2.38 Å). The adsorbed molecule forms two H bonds with two  $\text{O}_{1S}$  with a bond length of approximately 2 Å for all surfaces with the exception of the 1HB configuration of the  $\{111\}$  surface which has only one strong H bond (1.68 Å).

These common features lead us to conclude that the water adsorption is strongly affected by the surface Ce coordination which controls the  $\text{O}_W$  position and promotes the strong adhesion of the molecule while the H-bonding network with surface O atoms influences the orientation of the molecule. This is supported by the negligible difference in the adsorption energy between the 2HB and 1HB configurations of water on the  $\{111\}$  surface.

**3.3.2. Dissociative State at the Lowest Coverage.** The energetics of dissociative adsorption on the stoichiometric ceria surfaces when considering the lowest water coverage have been calculated to be  $-1.57$ ,  $-1.12$ , and  $-0.59$  eV for the  $\{100\}$ ,  $\{110\}$ , and  $\{111\}$  surfaces, respectively (Table 1). The order of the adsorption energies follows that of the stability of pure surfaces. Adsorption geometries of one dissociatively adsorbed water molecule are depicted in Figure 1 and arise from configurations in which the OH group and the H atom are in

the closest position with respect to each other within the symmetry of the surface.

On the type III {100} surface, the O<sub>W</sub>H<sub>W</sub> group has been placed on the oxygen vacant site left upon removal of half of the surface oxygen atoms and the configuration was maintained on relaxation (Figure 1b). No strong H bonding is present, as the shortest H<sub>W</sub>–O<sub>1S</sub> distance is approximately 2.50 Å. The Ce<sub>1S</sub>–OH distance is comparable to the Ce–O bulk distance. On the {110} surface, the O<sub>W</sub>H<sub>W</sub> relaxed 2.14 Å above the Ce<sub>1S</sub> with the proton residing on one of the O<sub>1S</sub> within the same oxygen coordination sphere (Figure 1d). The Ce<sub>1S</sub>–O<sub>1S</sub>H<sub>W</sub> distances are up to 8% longer than the bulk distance, as the proton is involved in the H bond with the O<sub>1S</sub> of the coordination sphere of the adjacent Ce<sub>1S</sub>. The position of the hydroxide at these two surfaces is dramatically different and explains the difference in the adsorption energies. Unlike at the {100} surface where two Ce<sub>1S</sub> gain stabilization sharing the hydroxyl group, at the {110} surface, only one Ce<sub>1S</sub> increases its coordination from 6 to 7 oxygen atoms. In the case of the {111} surface, the coordination of Ce<sub>1S</sub> is fully restored when an O<sub>W</sub>H<sub>W</sub> group is adsorbed 2.22 Å above Ce<sub>1S</sub> with an H adsorbed on the adjacent O<sub>1S</sub> (Figure 1g). One strong H bond was formed between the O<sub>1S</sub>H<sub>W</sub> and the O<sub>W</sub>H<sub>W</sub> (1.65 Å), while the Ce<sub>1S</sub>–O<sub>1S</sub>H<sub>W</sub> distance has stretched to 3.00 Å. The distance between the oxygen atoms of the hydroxyl groups is 2.55 Å which compares well with the distance of 2.52 Å previously reported.<sup>31</sup> The adsorption energy of dissociatively adsorbed water on the stoichiometric CeO<sub>2</sub>{111} surface is almost half of the value of the {110} surface even though only one Ce<sub>1S</sub> is stabilized by the hydroxyl group. We infer that in this case the difference in energy lies in the smaller oxygen coordination number of the Ce<sub>1S</sub> at the {110} compared with the {111} upon removal of the hydroxyl group. The calculated adsorption energy is also in agreement with other computational values of −0.53 eV<sup>31</sup> and of −0.55 eV.<sup>27</sup>

**3.3.3. Coverage Dependence of the Associative State on the Stoichiometric {111} Surface.** A remarkable experimental observation reported by Henderson et al.<sup>24</sup> indicated the presence of a strong coverage dependence of the desorption energy on the oxidized but not on the reduced CeO<sub>2</sub>(111) surface. Water underwent desorption at lower temperatures with increasing coverage on the oxidized surface, suggesting that at high coverage adsorption is destabilized relatively to low coverage. In our calculations, the adsorption energy (Table 1) decreases only by 0.01 eV when increasing the water coverage on the stoichiometric CeO<sub>2</sub>{111} surface and is −0.57 eV at 7.67H<sub>2</sub>O/nm<sup>2</sup> (1 ML) which compares well with the TPD desorption energy of 0.53 eV at the monolayer saturation.<sup>24</sup> Previous theoretical calculations also did not find coverage dependence. Kumar et al.<sup>26</sup> reported an increase of only 0.03 eV in the adsorption energy between 0.5 and 1 ML, while Fronzi et al.<sup>29</sup> calculated a reduction of 0.01 eV between 0.25 and 0.5 ML. The {111} surface geometry may be the reason for the lack of coverage dependence. The surface undergoes little relaxation so that the distances between atoms at the surface and in the bulk are similar. In our calculations, the surface O<sub>1S</sub>–O<sub>1S</sub> distance is 3.88 Å which corresponds also to the distance O<sub>W</sub>–O<sub>W</sub> of adjacent water molecules when considering the monolayer saturation. The surface area available for each molecule (13 Å<sup>2</sup>) is larger than the area occupied by the molecule itself (10 Å<sup>2</sup>) so that the interaction between molecules should be weak. In our 1 ML configuration, we do not see any H bonding between H<sub>2</sub>O molecules which are

approximately 3 Å apart. Each molecule can also only H-bond to one of the three available O<sub>1S</sub>, as each O<sub>1S</sub> can only donate one H bond. In this scenario, we infer that at this coverage H<sub>2</sub>O molecules do not gain any further stabilization due to H bonding as they are far apart. We also conclude that the change in the configuration of the adsorbate does not affect the energetics of the adsorption with increasing coverage because there is negligible energy (and Ce<sub>1S</sub>–O<sub>W</sub> distance) difference between the single and double H bond configurations at the lowest coverage. We are aware that our conclusions do not explain the shift of the TPD peak at lower temperatures when increasing the water coverage<sup>24</sup> unless we assume that the interchange between the 1HB and 2HB configurations is rapid and barrierless to cause profound disruption in the theoretical number of adsorbed molecules at the 1 ML saturation. For each double H bonded molecule, one adjacent adsorbed molecule needs to desorb. In this case, the coverage dependence arises from an average structure of the monolayer saturation which includes single and double H bond configurations with a different number of adsorbed molecules. This assumption also does not contradict SFM images of H<sub>2</sub>O on the stoichiometric CeO<sub>2</sub>(111) surface.<sup>20</sup>

**3.3.4. Coverage Dependence of the Associative State on the Stoichiometric {100} and {110} Surfaces.** We found that there is no significant coverage dependence for the associatively adsorbed water on the {100} and {110} surfaces, as the adsorption energy only increases by approximately 0.1 eV when increasing the coverage from 0.25 to 1 ML. At the {100} surface, the adsorption geometries for all water coverages studied are very similar. At the highest coverage which corresponds to the 1 ML coverage, associatively adsorbed water orientates with the H<sub>W</sub> pointing 14° outward from the surface plane, forming two H bonds (H<sub>W</sub>–O<sub>1S</sub> = 1.77–1.85 Å) and with the O<sub>W</sub> at 2.57 Å above Ce<sub>1S</sub>. Unlike at the {111} surface, at the {100} surface, each O<sub>1S</sub> can donate two H bonds, and therefore, at the monolayer saturation, water can still have a double H bond configuration saturating all possible H bonds. The adsorbed geometry at the highest 4.69 H<sub>2</sub>O/nm<sup>2</sup> coverage on the {110} surface has been found to be similar to the lowest, but the water is slightly rotated with a short H bond of 1.76 Å and a long one of 2.21 Å. Interestingly, the Ce<sub>1S</sub>–O<sub>W</sub> distance is 2.58 Å which is very close to the Ce–O<sub>W</sub> distance at all coverage on all surfaces.

**3.3.5. Coverage Dependence of the Dissociative State.** Coverage dependence is seen when considering dissociative water adsorption (Table 1). The {100} surface shows the largest variation in the adsorption energy with 0.68 eV difference between the highest and lowest coverage with the latter being more stable. At the highest coverage, every oxygen vacant site created during the removal of the dipole on the stoichiometric surface is filled by a hydroxide so that the surface oxygen layer and the 8-fold coordination of all Ce<sub>1S</sub> are fully restored. However, there is no gain in stabilization arising from the H-bonding network. An additional coverage (0.5 ML or 3.32 H<sub>2</sub>O/nm<sup>2</sup>) has been studied with the hydroxyl groups in all the possible configurations. The adsorption energy has been found to vary from −1.73 to −0.87 eV, and the difference between those configurations is the presence of H bonds with the most stable having two H bonds (1.79 Å) and the least having none.

Unlike the {100} surface, the {110} surface shows the smallest increase in the adsorption energy (0.12 eV) when increasing the water coverage to 1 ML. At the 4.69 H<sub>2</sub>O/nm<sup>2</sup>

(1 ML) coverage, OH groups are in the same position and orientation as described for the lowest coverage with the Ce<sub>1S</sub>–O<sub>W</sub>H<sub>W</sub> and Ce<sub>1S</sub>–O<sub>1S</sub>H<sub>W</sub> distances of 2.14 and 2.48 Å, respectively, and a very weak H bond (2.39 Å). At this coverage, all Ce<sub>1S</sub> are 7-coordinated, and in order to clarify if a fully restored coordination of surface Ce ions destabilizes the structure, we performed the 9.39 H<sub>2</sub>O/nm<sup>2</sup> coverage which according to the common definition of a monolayer (one H<sub>2</sub>O per Ce atom) would be the 2 ML. In this fully hydroxylated surface, all Ce<sub>1S</sub> are 8-fold coordinated, but the adsorption energy dropped at a value of −0.21 eV.

A quite strong water coverage dependence is also shown at the {111} surface with the highest coverage (1 ML) being destabilized of 0.44 eV (Table 1) compared to the lowest coverage (0.17 ML). As for the single dissociatively adsorbed water, the O<sub>W</sub>H<sub>W</sub> group is on top of the Ce<sub>1S</sub> (2.20 Å) and the proton is bonded to the closest O<sub>1S</sub>. Unlike the surface with a single dissociatively adsorbed molecule, the fully hydroxylated surface does not show any stabilization due to H bond formation.

**3.3.6. Associative and Dissociative States within the Coverage Dependence.** The results clearly show that the dissociative state is the thermodynamically most stable state for the {100} and {110} ceria surfaces. The small differences in adsorption energy (0.01 eV) found for the {111} surface indicate that H<sub>2</sub>O molecules and hydroxyl groups are both accessible at low coverage.<sup>20,21</sup> No literature data are available for the {100} and {110} surfaces, while there is a discrepancy within computational results for the energetically most stable state on the stoichiometric {111} ceria surface. Dissociation of water was found favorable in one case with an adsorption energy of −0.53 eV,<sup>31</sup> while in the other the associative state was favored by 0.13 eV<sup>29</sup> and by 0.02 eV<sup>27</sup> with respect to the dissociative state. *Ab initio* MD was also performed to address the issue, and the result supports the dissociation of the molecule at room temperature.<sup>30,31</sup>

Interestingly, the stability of the dissociative state decreases with increasing amount of hydroxyl groups, particularly when the 8-fold coordination of surface Ce atoms is fully restored. For intermediate (3.32 H<sub>2</sub>O/nm<sup>2</sup>) coverage, the adsorption energy ranges between −1.73 and −0.87 eV for the {100} surface, where the H-bonding network plays an important role in the stabilization. The stability of the associative state depends on which surface is considered. At the {110} surface, the dissociative state is always energetically more stable than the associative state, while the {100} surface seems to have no preference toward the two states at high water coverage but the dissociative is more stable than the associative at low coverage. At the {111} surface, there is no significant change in the adsorption energy of the associative state with increasing water coverage. The associative state is more stable than the dissociative state at higher coverage while equally accessible at low coverage. At the 7.67 H<sub>2</sub>O/nm<sup>2</sup> coverage, both associative and dissociative adsorptions have energy lower than −0.60 eV in agreement with the TPD desorption peaks being below RT and suggesting no irreversibly adsorbed water.<sup>24</sup> The coverage dependence of the dissociative state can however provide an explanation to the shift in the TPD peak as both associative and dissociative states are present for low coverage, but when the water coverage increases, the dissociative state becomes destabilized and hence the shift of the TPD peak.<sup>24</sup>

**Table 3. Adsorption Energies of Associatively (H<sub>2</sub>O) and Dissociatively (H–OH) Adsorbed Water on the Reduced Ceria Surfaces for the Lowest Water Coverage (H<sub>2</sub>O/nm<sup>2</sup>)** (§ above the Vo; \*above the Ce; #not above the Vo)

		Adsorption Energy (eV)
{100}	H–OH	−2.54
	H <sub>2</sub> O	−0.87 <sup>#</sup>
{110}	H–OH	−1.44
	H <sub>2</sub> O	N/A
{111}	H–OH	−2.12
	H <sub>2</sub> O	−0.82* (−0.58 <sup>§</sup> )

**3.4. Water Adsorption on Reduced {100}, {110}, and {111} Ceria Surfaces.** Turning now to the adsorption of water at reduced surfaces, we have calculated the energetics of the associative and dissociative adsorption at or near an oxygen vacancy.

Associatively adsorbed water at the reduced {111} surface has adsorption energies of −0.82 and −0.58 eV (Table 3) at the 1.28 H<sub>2</sub>O/nm<sup>2</sup> (1.7 ML) coverage for water above Ce<sub>1S</sub> (Figure 2d) and Vo (Figure 2e), respectively. For the most stable configuration, the molecule is adsorbed 2.62 Å above the Ce<sub>1S</sub> slightly shifted toward the Vo forming one H bond with O<sub>1S</sub> (1.53 Å). For this configuration, Fronzi et al.<sup>29</sup> calculate an adsorption energy of −0.59 eV (0.25 ML) arguing however that

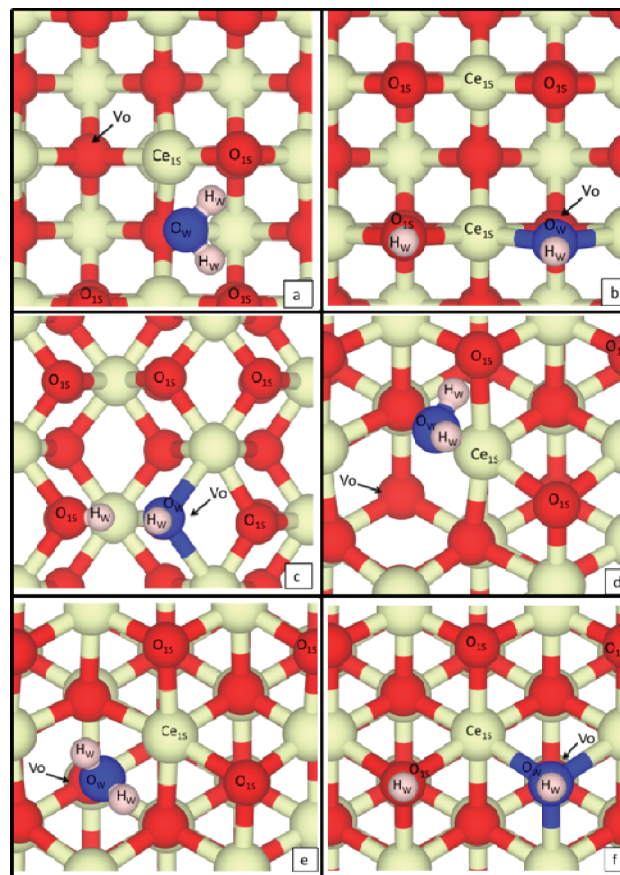


**Figure 2.** Top view of the adsorption site of associatively adsorbed water on (a) {100} and (d and e) {111} and dissociatively adsorbed water (b) {100}, (c) {110}, and (f) {111} reduced ceria surfaces. White, red, pink, and blue spheres are Ce, O, H<sub>w</sub>, and O<sub>w</sub> atoms, respectively.

the most stable adsorption geometry has the water molecule residing above the Vo ( $-1.28$  eV). The latter configuration is also reported by Watkins et al.<sup>31</sup> and Marrocchelli et al.<sup>30</sup> (DFT-GGA+U) with a lower adsorption energy of  $-0.79$  eV (0.5 ML) and  $-0.8$  eV, respectively. Contrary to these results, Kumar et al.<sup>26</sup> report that water prefers to adsorb above  $\text{Ce}_{1s}$  with adsorption energies ranging between  $-0.55$  and  $-0.64$  eV (0.5 ML). When considering the dissociative state, we found that the adsorption is thermodynamically more favorable than that of water in the associative state of  $1.30$  eV (Table 3). Two surface OH groups are formed with  $\text{O}_w$  occupying the Vo (Figure 2f). The proton resides on the adjacent  $\text{O}_{1s}$ , and the  $\text{Ce}_{1s}-\text{OH}$  distances range between  $2.59$  and  $2.64$  Å. The present result is in agreement with both Watkins et al.<sup>31</sup> and Fronzi et al.<sup>29</sup> that found the adsorption energy of the dissociative state to be  $-2.45$  and  $-1.40$  eV, respectively, and with the SFM images of Gritschneider et al.<sup>21</sup>

The  $\{100\}$  surface has similar behavior to the  $\{111\}$  surface. The water molecule adsorbs (Figure 2a) in the same position as for the stoichiometric surface with longer  $\text{Ce}_{1s}-\text{O}_w$  distances of approximately  $2.80$  Å and stronger H bonds with bond lengths ranging between  $1.57$  and  $1.74$  Å. The dissociative state is  $1.66$  eV more stable than the associative state with the hydroxyl groups at approximately  $2.44$  Å from the  $\text{Ce}_{1s}$  and no H bonds. Unlike at the  $\{100\}$  and  $\{111\}$  surfaces, dissociation of water occurred during minimization when  $\text{H}_2\text{O}$  is above the Vo on the  $\{110\}$  surface (Figure 2c), suggesting that the energy barrier of dissociation is negligible. The  $\text{Ce}_{1s}-\text{OH}$  distances range between  $2.50$  and  $2.70$  Å, and one H bond is formed between the OH groups with a bond length of  $1.80$  Å. The energy of adsorption is  $-1.44$  eV.

It is well-known that the presence of oxygen vacancies can be compensated by  $\text{Ce}^{3+}$  ions in the lattice. This can be revealed by using the total density of states (TDOS) which we report only for the  $\{111\}$  surface as an example. Indeed, TDOS of all surfaces show the  $\text{Ce}^{3+}$  as a gap state which is circled in Figure 3b for the  $\{111\}$  reduced surface, but it is clearly absent in the stoichiometric surface (Figure 3a). However, with dissociative adsorption of water, the Vo is removed but the positive charge remains. This means that the presence of  $\text{Ce}^{3+}$  ions does not imply the existence of  $\text{Vo}^{24,25}$  when water is present and this will not be trivial when considering nanoparticles with large surface areas. Figure 3 shows a comparison between the TDOS of the  $\{111\}$  stoichiometric and reduced surface in the presence of associatively and dissociatively adsorbed water. The TDOS for reduced surfaces show the  $\text{Ce}^{3+}$  gap state both when the Vo is exposed interacting with the water molecule (Figure 3d) and when Vo is healed by hydroxyl groups (Figure 3f).

**3.5. Reduced  $\{100\}$ ,  $\{110\}$ , and  $\{111\}$  Ceria Surfaces in the Presence of the Water Solvent.** Table 4 shows the heat of reduction of ceria surfaces in the presence of water. R-A and R-D refer to the stoichiometric surface (reactant R), and P-A and P-D refer to the final reduced configuration (product P) with associatively (A) and dissociatively (D) adsorbed water, respectively. We consider the reaction between the most thermodynamically stable states, and therefore, the significant reaction is R-D/P-D for all surfaces. However, as we have found associatively adsorbed water on ceria  $\{100\}$  and  $\{111\}$  reduced surfaces, we also include the reaction R-A/P-A. The heat of reduction has been calculated as in eq 3, where  $E(\text{CeO}_{2-x} + \text{W})$  and  $E(\text{CeO}_2 + \text{W})$  are the energies of the reduced and stoichiometric slabs with dissociatively or associatively adsorbed water (W) and  $E(\text{O}_2)$  is the binding energy of the  $\text{O}_2$  gas phase

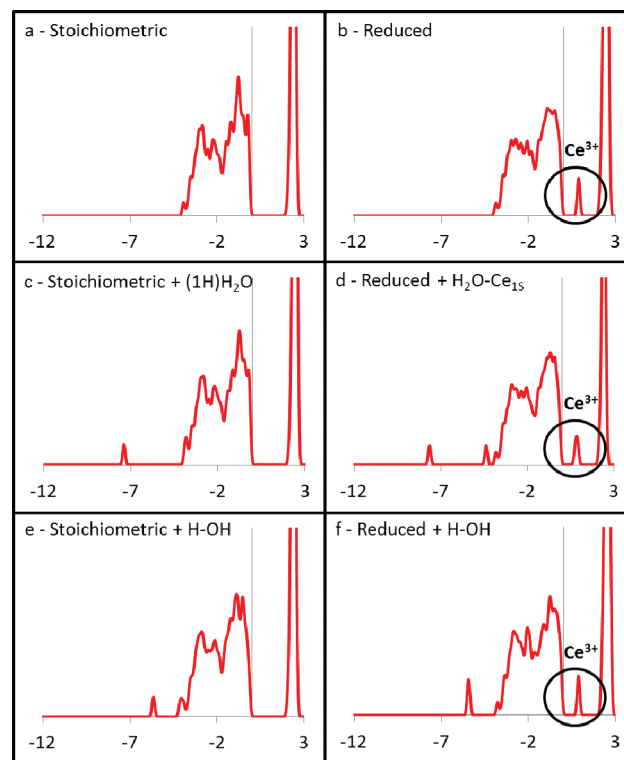


**Figure 3.** TDOS vs energy (eV) of  $\{111\}$  stoichiometric and reduced ceria surfaces in the absence of water (a and b) and in the presence of associatively and dissociatively adsorbed water (c and d) and (e and f), respectively. Water has a 1H bond in (c) and is above  $\text{Ce}_{1s}$  in (d).  $\text{Ce}^{3+}$  as a gap state is circled.

**Table 4. Heat of Reduction of Ceria Surfaces in the Presence of Water (§ above the Vo; \*above the Ce; #not above the Vo)**

	Heat of Reduction (eV)	
	R-A/P-A	R-D/P-D
{100}	1.74 <sup>#</sup>	0.63 <sup>#</sup>
{110}	N/A	0.97
{111}	1.77* (2.01 <sup>§</sup> )	0.48

molecule in its triplet state. R-D/P-D and R-A/P-A are then the reactions which include water in the dissociative and associative states, respectively, in both the reduced and stoichiometric surfaces.

$$E_{\text{red}} = [E(\text{CeO}_{2-x} + \text{W}) + E(\text{O}_2) - E(\text{CeO}_2 + \text{W})]/2 \quad (3)$$

The results in Table 4 show that creating Vo in the presence of water is energetically more favorable than removing an oxygen ion from a dry surface. The cost of creating Vo on the wet stoichiometric  $\{111\}$  surface has been calculated to be  $0.48$  eV when the initial and final states are dissociative, which is  $1.53$  eV lower than the heat of reduction of the dry surface. This decrease was previously reported<sup>26,29</sup> but does not explain why there is no significant shift in temperature in the desorption peak of the TPD spectra promoted by the presence of oxygen vacancies which might imply different stabilization mechanisms.<sup>24</sup> We have also included the heat of reduction for the reaction R-A/P-A as Gritschneider et al.<sup>21</sup> showed the presence of water molecules on oxygen vacancies. For the two final associative states, one with the water above the  $\text{Ce}_{1s}$  and one above the Vo, we calculated values of heat of reduction of  $1.77$

**Table 5.** Temperature of Desorption of Associatively ( $\text{H}_2\text{O}$ ) and Dissociatively ( $\text{H}-\text{OH}$ ) Adsorbed Water on Stoichiometric and Reduced Surfaces of Ceria

	{100}		Temperature of Desorption (K)		{111}	
	$\text{H}_2\text{O}$	$\text{H}-\text{OH}$	$\text{H}_2\text{O}$	$\text{H}-\text{OH}$	$\text{H}_2\text{O}$	$\text{H}-\text{OH}$
$p = 10^{-12} \text{ bar}$						
stoichiometric	250–275	400–425	200–225	275–300	150–175	150–175
reduced	200–225	575–600	200–225	350–375	200–225	500–525
$p = 10^{-10} \text{ bar}$						
stoichiometric	275–300	475–500	250–275	300–325	175–200	175–200
reduced	250–275	400–425	250–275	400–425	225–250	550–575
$p = 1 \text{ bar}$						
stoichiometric	525–550	825–850	450–475	575–600	325–350	325–350
reduced	450–475	>1000	450–475	725–750	425–450	>1000

and 2.01 eV, respectively (Table 4). Both values are not as favorable as in the case of considering the dissociative final state.

For the wet {110} surface, the heat of reduction is 0.97 eV (R-D/P-D) which is only 0.32 eV more favorable than that of the dry surface. For this surface, the reaction R-A/P-A cannot be calculated as we found dissociation of water on the reduced surface during minimization. The heat of reduction of the {100} surface shows a remarkable value of 0.63 eV. However, when considering the reaction R-A/P-A, the heat of reduction becomes less favorable than that of the dry surface. This can be explained by the fact that the associative final state is far less stable than the dissociative state (Table 3) and therefore water might split during adsorption.

**3.6. Thermodynamics of Desorption.** Finally, we investigated the stability of ceria surfaces in equilibrium with an atmosphere of gaseous water at temperature  $T$ . We followed the approach of Sun et al.<sup>58</sup> and more recently Kerisit et al.<sup>59</sup> who considered the influence of water and  $\text{CO}_2$  on calcite. For both stoichiometric and reduced surfaces, we include the influence of water, but for the reduced surfaces, we do not include the contribution of the oxygen partial pressure on the variation of the free energy. We calculate the surface energy when water is adsorbed on ceria surface at different  $T$ , as shown in eq 4 where  $C$  is the coverage (molecules  $\text{m}^{-2}$  mol),  $E_{\text{ads}}$  is the adsorption energy as in eq 2,  $(G_{\text{water}} - \text{ZPE})$  is the Gibbs free energy of water purged of the zero point energy,  $R$  is the gas constant,  $T$  is the temperature, and  $p$  and  $p^\circ$  are the partial pressures of water chosen and in the standard state (1 bar), respectively.

$$\gamma_{(\text{wet}, T, p)} = \gamma_{(\text{dry})} + (C(E_{\text{ads}} - (G_{\text{water}} - \text{ZPE}) - RT \ln(p/p^\circ))) \quad (4)$$

The results enable us to evaluate the surface free energies as a function of water chemical potential, and we can calculate, for example, the temperature of which water desorbs from surfaces (Table 5).

At a pressure of  $10^{-10}$  bar, hydrated and hydroxylated stoichiometric {111} surfaces are more stable than the dry surface up to 175–200 K, which is in good agreement with the experimental study of Matolin et al.<sup>25</sup> on water desorption on the  $\text{CeO}_2(111)$  surface grown on a  $\text{Cu}(111)$  surface where 170–185 K was reported as the desorption temperature range for the single water layer. As the water in the associative and dissociative states desorbs at the same temperature, we can also

infer that the concentrations of  $\text{H}_2\text{O}$  and  $\text{OH}$  converge to the same value after 200 K. Beyond this temperature, water does not adsorb on the {111} surface. Between 120 and 200 K, a much higher concentration of associatively adsorbed water was found,<sup>25</sup> which agrees with the thermodynamic higher stability of water in the associative state at the monolayer saturation. The situation is predicted to be the same for the reduced {111} surface where associatively adsorbed water is present at the surface up to 200 K. However, dissociatively adsorbed water is calculated to be present up to 575 K, implying that the concentration of OH groups will be higher than that of  $\text{H}_2\text{O}$  between 250 and 575 K, as also shown by the experiments.<sup>25</sup> This finding supports the view that the oxygen vacancy can act as a reactive site, as water will prefer the most thermodynamically stable dissociative state (Table 3).

Below 225 K, water may be present in the associative state on the {111} reduced surface even though the adsorption energy is higher than that of the dissociative state, as dissociation might be kinetically unfavorable at these temperatures. However, above 250 K, the dissociation might become favorable as the concentration of OH is higher than that of  $\text{H}_2\text{O}$ . At a pressure of about  $10^{-12}$  bar, TPD spectra from Henderson et al.<sup>24</sup> show desorption peaks between 195 and 265 K depending on the water coverage on the oxidized  $\text{CeO}_2(111)$  surface grown on the YSZ(111) surface. At the 0.20 ML water coverage, the temperature of desorption is found to be 265 K, which is higher than our calculated temperature of 150–175 K at the 0.17 ML water coverage but lower than the 350 K at the 0.25 ML water coverage calculated by Fronzi et al.<sup>29</sup> which included the oxygen chemical potential. The presence of a reduced surface increases the temperature of desorption of about 50 K when considering the associative state and 350 K in the presence of hydroxyl groups. The large experimental range of desorption temperatures may be indicative of the presence of different surface elements on the  $\text{CeO}_2(111)$  surface due to the different conditions during the synthesis and the analysis and the different supports used to grow the sample while in our calculation we have a perfect {111} surface.

Desorption temperatures for the {100} and {110} surfaces have not been reported experimentally to our knowledge. Here we predict that, at ultrahigh vacuum pressures (Table 5), associatively adsorbed water at the stoichiometric {100} and {110} surfaces desorbs above 275 and 225 K, respectively, while dissociatively adsorbed water desorbs above 425 and 300 K, respectively. When considering the reduced {100} surface, the dissociative state has a much higher temperature of desorption (575–600 K) compared to the associative state

(200–225 K). Dissociatively adsorbed water at the reduced {110} surface desorbs at lower temperature (350–375 K), while associatively adsorbed water desorbs in the same range of temperature for the {100} surface.

This trend can also be seen at 1 bar, as shown in Table 5. Reduced surfaces show higher temperatures of desorption than stoichiometric surfaces with the only exception of the associative state on the {100} surface. Water in the associative state tends also to desorb at lower temperatures compared to water in the dissociative state except for the {111} surface where the values are identical.

#### 4. CONCLUSIONS

We have calculated the energetics and predicted the geometry of adsorbed water molecules on the stoichiometric and reduced low index {100}, {110}, and {111} surfaces of ceria comparing the results, where available, with experimental data and previous theoretical calculations.

Our detailed systematic study reveals that the dissociative state at low water coverage is always thermodynamically more favorable than the associative state on all stoichiometric and reduced surfaces with only one exception, namely, the {111} surface where both are equally accessible. The adsorption geometries are strongly affected by the coordination of surface cerium atoms, while the orientation of the adsorbate is likely to be more affected by the H bonding network between surface oxygen atoms and the water molecule. There is weak coverage dependence for associatively adsorbed water on the stoichiometric {100} and {110} surfaces, and it is negligible for the {111} surface which is due to a lack of interactions among adsorbed water molecules on the surface. In contrast, there is strong water coverage dependence for dissociatively adsorbed water on all stoichiometric surfaces. On the reduced surfaces, the presence of oxygen vacancies increases the adsorption energy favoring the dissociative state. For the {110} surface, dissociation is predicted to be barrierless. The heat of reduction of wet surfaces is lower than that of dry surfaces. This implies that the reduced surface is always stabilized by the presence of water which needs to be taken into account when studying the catalytic properties of ceria. The presence of Ce<sup>3+</sup> can then be correlated with the presence of oxygen vacancies and hydroxyl groups, and hence, we suggest that the resulting defects will affect the redox properties of ceria even more when considering nanostructures with high surface area. Finally, the pressures and temperatures of desorption of water have been predicted. The simulations predict that hydroxyl groups desorb at higher temperature compared to associatively adsorbed water; this implies, for example, that water gas shift catalysts working at atmospheric pressure (about 1 bar) in an intermediate range of temperatures (400–600 K) have to face the presence of OH groups. The temperatures of desorption show a marked shift toward high temperature when moving from stoichiometric to reduced surfaces, and the results suggest that this can therefore be used experimentally to discriminate the same sample of ceria in the oxidized and reduced state.

#### AUTHOR INFORMATION

##### Corresponding Author

\*E-mail: s.c.parker@bath.ac.uk.

##### Notes

The authors declare no competing financial interest.

#### ACKNOWLEDGMENTS

EPSRC: EP/H005838/1 and EP/H001220/1 for funding. Computations were run on HPC Aquila at the University of Bath and HECToR facilities through the Materials Chemistry Consortium.

#### REFERENCES

- (1) Campbell, C. T.; Peden, C. H. F. *Science* **2005**, *309*, 713–714.
- (2) Esch, F.; Fabris, S.; Zhou, L.; Montini, T.; Africh, C.; Fornasiero, P.; Comelli, G.; Rosei, R. *Science* **2005**, *309*, 752–755.
- (3) Cargnello, M.; Gentilini, C.; Montini, T.; Fonda, E.; Mehraeen, S.; Chi, M.; Herrera-Collado, M.; Browning, N. D.; Polizzi, S.; Pasquato, L.; et al. *Chem. Mater.* **2010**, *22*, 4335–4345.
- (4) Barreca, D.; Gasparotto, A.; Maccato, C.; Maragno, C.; Tondello, E. *Langmuir* **2006**, *22*, 8639–8641.
- (5) Lu, Z. Y.; Ryde, N. P.; Babu, S. V.; Matijevic, E. *Langmuir* **2005**, *21*, 9866–9872.
- (6) Suratwala, T. I.; Feit, M. D.; Steele, W. A. *J. Am. Ceram. Soc.* **2010**, *93*, 1326–1340.
- (7) Park, S. D.; Vohs, J. M.; Gorte, R. J. *Nature* **2000**, *404*, 265–267.
- (8) Dresselhaus, M. S.; Thomas, I. L. *Nature* **2001**, *414*, 332–337.
- (9) Malavasi, L.; Fisher, C. A. J.; Islam, M. S. *Chem. Soc. Rev.* **2010**, *39*, 4370–4387.
- (10) Tarnuzzer, R. W.; Colon, J.; Patil, S.; Seal, S. *Nano Lett.* **2005**, *5*, 2573–2577.
- (11) Karakoti, A. S.; Singh, S.; Kumar, A.; Malinska, M.; Kuchibhatla, S. V. N. T.; Wozniak, K.; Self, W. T.; Seal, S. *J. Am. Chem. Soc.* **2009**, *131*, 14144–14145.
- (12) Zhang, J.; Kumagai, H.; Yamamura, K.; Ohara, S.; Takami, S.; Morikawa, A.; Shinjoh, H.; Kaneko, K.; Adschiri, T.; Suda, A. *Nano Lett.* **2011**, *11*, 361–364.
- (13) Yang, S.; Gao, L. *J. Am. Chem. Soc.* **2006**, *128*, 9330–9331.
- (14) Tyrsted, C.; Becker, J.; Hald, P.; Bremholm, M.; Pedersen, J. S.; Chevallier, J.; Cerenius, Y.; Iversen, S. B.; Iversen, B. B. *Chem. Mater.* **2010**, *22*, 1814–1820.
- (15) Otsuka, K.; Hatano, M.; Morikawa, A. *J. Catal.* **1983**, *79*, 493–496.
- (16) Padeste, C.; Cant, N. W.; Trimm, D. L. *Catal. Lett.* **1993**, *18*, 305–316.
- (17) Kundakovic, L.; Mullins, D. R.; Overbury, S. H. *Surf. Sci.* **2000**, *457*, 51–62.
- (18) Berner, U.; Schierbaum, K.; Jones, G.; Wincott, P.; Haq, S.; Thornton, G. *Surf. Sci.* **2000**, *467*, 201–213.
- (19) Hayun, S.; Shvareva, T. Y.; Navrotsky, A. *J. Am. Ceram. Soc.* **2011**, *94*, 3992–3999.
- (20) Gritschneider, S.; Iwasawa, Y.; Reichling, M. *Nanotechnology* **2007**, *18*, 044025.
- (21) Gritschneider, S.; Reichling, M. *Nanotechnology* **2007**, *18*, 044024.
- (22) Senanayake, S. D.; Stacchiola, D.; Evans, J.; Estrella, M.; Barrio, L.; Perez, M.; Hrbek, J.; Rodriguez, J. A. *J. Catal.* **2010**, *271*, 392–400.
- (23) Mullins, D. R.; Radulovic, P. V.; Overbury, S. H. *Surf. Sci.* **1999**, *429*, 186–198.
- (24) Henderson, M. A.; Perkins, C. L.; Engelhard, M. H.; Thevuthasan, S.; Peden, C. H. F. *Surf. Sci.* **2003**, *526*, 1–18.
- (25) Matolín, V.; Matolínová, I.; Dvořák, F.; Johánek, V.; Mysliveček, J.; Prince, K. C.; Skála, T.; Stetsovyč, O.; Tsud, N.; Václavů, M.; et al. *Catal. Today* **2011**, *181*, 124–132.
- (26) Kumar, S.; Schelling, P. K. *J. Chem. Phys.* **2006**, *125*, 204704.
- (27) Yang, Z.; Wang, Q.; Wei, S.; Ma, D.; Sun, Q. *J. Phys. Chem. C* **2010**, *114*, 14891–14899.
- (28) Chen, H.-T.; Choi, Y. M.; Liu, M.; Lin, M. C. *ChemPhysChem* **2007**, *8*, 849–855.
- (29) Fronzi, M.; Piccinin, S.; Delley, B.; Traversa, E.; Stampfl, C. *Phys. Chem. Chem. Phys.* **2009**, *11*, 9188–9199.
- (30) Marrocchelli, D.; Yildiz, B. *J. Phys. Chem. C* **2011**, *116*, 2411–2424.

- (31) Watkins, M. B.; Foster, A. S.; Shluger, A. L. *J. Phys. Chem. A* **2007**, *111*, 15337–15341.
- (32) Kresse, G.; Hafner, J. *Phys. Rev. B* **1994**, *49*, 14251–14269.
- (33) Kresse, G.; Furthmuller, J. *Phys. Rev. B* **1996**, *54*, 11169–11186.
- (34) Blochl, P. E. *Phys. Rev. B* **1994**, *50*, 17953–17979.
- (35) Kresse, G.; Joubert, D. *Phys. Rev. B* **1999**, *59*, 1758–1775.
- (36) Perdew, J. P.; Burke, K.; Ernzerhof, M. *Phys. Rev. Lett.* **1996**, *77*, 3865–3868.
- (37) Dudarev, S. L.; Botton, G. A.; Savrasov, S. Y.; Humphreys, C. J.; Sutton, A. P. *Phys. Rev. B* **1998**, *57*, 1505–1509.
- (38) Anisimov, V. I.; Zaanen, J.; Andersen, O. K. *Phys. Rev. B* **1991**, *44*, 943–954.
- (39) Nolan, M.; Parker, S. C.; Watson, G. W. *Surf. Sci.* **2005**, *595*, 223–232.
- (40) Nolan, M.; Grigoleit, S.; Sayle, D. C.; Parker, S. C.; Watson, G. W. *Surf. Sci.* **2005**, *576*, 217–229.
- (41) Keating, P. R. L.; Scanlon, D. O.; Watson, G. W. *J. Phys.: Condens. Matter* **2009**, *21*, 405502–6.
- (42) Scanlon, D. O.; Galea, N. M.; Morgan, B. J.; Watson, G. W. *J. Phys. Chem. C* **2009**, *113*, 11095–11103.
- (43) Scanlon, D. O.; Morgan, B. J.; Watson, G. W. *Phys. Chem. Chem. Phys.* **2011**, *13*, 4279–4284.
- (44) Oliver, P. M.; Parker, S. C.; Mackrodt, W. C. *Modell. Simul. Mater. Sci. Eng.* **1993**, *1*, 755–760.
- (45) Momma, K.; Izumi, F. *J. Appl. Crystallogr.* **2008**, *41*, 653–658.
- (46) Tasker, P. W. *J. Phys. C: Solid State Phys.* **1979**, *12*, 4977–4984.
- (47) Oliver, P. M.; Watson, G. W.; Parker, S. C. *Phys. Rev. B* **1995**, *52*, 5323–5329.
- (48) Sims, J. R.; Blumenthal, R. N. *High Temp. Sci.* **1976**, *8*, 99–110.
- (49) Skorodumova, N. V.; Baudin, M.; Hermansson, K. *Phys. Rev. B* **2004**, *69*, 075401–8.
- (50) Sayle, T. X. T.; Parker, S. C.; Catlow, C. R. A. *J. Phys. Chem.* **1994**, *98*, 13625–13630.
- (51) Balducci, G.; Kaspar, J.; Fornasiero, P.; Graziani, M.; Islam, M. *S. J. Phys. Chem. B* **1998**, *102*, 557–561.
- (52) Sayle, T. X. T.; Parker, S. C.; Sayle, D. C. *Chem. Commun.* **2004**, 2438–2439.
- (53) Barnard, A. S.; Kirkland, A. I. *Chem. Mater.* **2008**, *20*, 5460–5463.
- (54) Sayle, T. X. T.; Inkson, B. J.; Karakoti, A.; Kumar, A.; Molinari, M.; Moebus, G.; Parker, S. C.; Seal, S.; Sayle, D. C. *Nanoscale* **2011**, *3*, 1823–1837.
- (55) Yang, Z. X.; Woo, T. K.; Baudin, M.; Hermansson, K. *J. Chem. Phys.* **2004**, *120*, 7741–7749.
- (56) Nolan, M.; Fearon, J. E.; Watson, G. W. *Solid State Ionics* **2006**, *177*, 3069–3074.
- (57) Tuller, H. L.; Nowick, A. S. *J. Electrochem. Soc.* **1979**, *126*, 209–217.
- (58) Sun, Q.; Reuter, K.; Scheffler, M. *Phys. Rev. B* **2003**, *67*, 205424–7.
- (59) Kerisit, S.; Marmier, A.; Parker, S. C. *J. Phys. Chem. B* **2005**, *109*, 18211–18213.